HHS Public Access

Author manuscript

Org Lett. Author manuscript; available in PMC 2020 September 13.

Published in final edited form as:

Org Lett. 2019 September 20; 21(18): 7577–7581. doi:10.1021/acs.orglett.9b02856.

Characterization by Empirical and Computational Methods of Dictyospiromide, an Intriguing Antioxidant Alkaloid from the Marine Alga *Dictyota coriacea*

Pengcheng Yan[*,†], **Ge Li**[†], **Chaojie Wang**[†], **Jianzhang Wu**[*,†], **Zhongmin Sun**[‡], **Gary E. Martin**[§], **Xiao Wang**[‖], **Mikhail Reibarkh**[‖], **Josep Saurí**[⊥], **Kirk R. Gustafson**[*,#]

[†]School of Pharmaceutical Sciences, Wenzhou Medical University, Wenzhou, Zhejiang 325035, People's Republic of China

[‡]Institute of Oceanology, Chinese Academy of Sciences, Qingdao 266071, People's Republic of China

[§]Department of Chemistry and Biochemistry, Seton Hall University, South Orange, New Jersey 07079, United States

[‖]Structure Elucidation Group, Analytical Research and Development, Merck & Co., Rahway, New Jersey 07065, United States

[⊥]Structure Elucidation Group, Analytical Research and Development, Merck & Co., Boston, Massachusetts 02115, United States

[#]Molecular Targets Program, Center for Cancer Research, National Cancer Institute, Frederick, Maryland 21702, United States

ABSTRACT:

The challenging structural motif of dictyospiromide (**1**), a spirosuccinimide alkaloid with antioxidant properties that are associated with activation of the Nrf2/ARE signaling pathway, was assigned using contemporary NMR experiments complemented with anisotropic NMR, chiroptical, and computational methodologies. Anisotropic NMR parameters provided critical orthogonal verification of the configuration of the difficult to assign spiro carbon and the other stereogenic centers in **1**.

Graphical Abstract

[*]**Corresponding Authors** gustafki@mail.nih.gov., yanpc@wmu.edu.cn., wujianzhang@wmu.edu.cn.

ASSOCIATED CONTENT

Supporting Information

The Supporting Information is available free of charge on the ACS Publications website at DOI: 10.1021/acs.or-glett.9b02856.

Experimental procedures, spectroscopic data, and computational methods for dictyospiromide (**1**) (PDF)

The authors declare no competing financial interest.

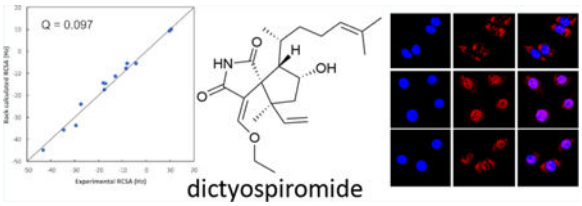

Recent advances in spectroanalytical techniques and computational methods have improved the accuracy and ability to make structure assignments for small molecules of unknown constitution. These advanced capabilities are particularly important in the structural definition of new natural products, which often contain novel molecular architecture and functional group arrays. NMR experiments utilizing newly developed pulse sequences have provided additional tools for structure elucidation,[1] while modifications in 2D data acquisition and processing such as nonuniform sampling (NUS) techniques increase both the resolution and sensitivity of these experiments.[2] In addition to conventional NMR approaches, anisotropy-based NMR measurements of residual dipolar coupling (RDC) and residual chemical shift anisotropy (RCSA) provide an orthogonal means to define and confirm both the structural framework and configuration of new compounds.[3] Improved quantum mechanics based computational methods such as density functional theory (DFT) calculations of chemical shifts,[4] coupling constants,[5] chiroptical properties,[6] and anisotropy parameters[7] can be employed in combination with experimental spectroscopic measurements to define challenging structures that previously required an alternative approach such as X-ray analysis or synthesis.[3e,f]

Marine brown algae of the genus *Dictyota* are a rich source of unusual diterpenes with diverse skeletons, many of which are biologically active.[8] The potential of these metabolites as cytoprotectants against oxidative stress has generally not been evaluated, so specimens of *Dictyota coriacea* from the East China Sea were collected and analyzed. Fractionation of the EtOAc extract provided a diterpenoid metabolite with a unique carbon and nitrogen structural scaffold (Figure 1a) that was named dictyospiromide (**1**). Compound **1** had a molecular formula of $C_{22}H_{33}NO_4$ based on HRMS data, which required seven degrees of unsaturation. The ^{13}C NMR spectrum displayed 22 carbon signals including two carbonyls and six additional sp^2 carbons, which indicated that **1** was bicyclic. Comprehensive 1D and 2D NMR analysis (see the Supporting Information for details) allowed assignment of a substituted 2-azaspiro[4.4]nonane-1,3-dione moiety for dictyospiromide (**1**), which represents a novel diterpenoid skeleton.

The relative configurations at C-3, C-4, C-6, and C-10 in **1** were determined by NOESY analysis (Figure 1b). NOESY correlations between H-3/H_3-17, H-4/H_3-17, and 4-OH/H-10 suggested the 3*S**,4*R**,10*R** configuration—the latter was also supported by an observed NOE between H-9/H-11a/b, while a correlation between H-7/H-3 was indicative of 6*S**. The large coupling (12.0 Hz) between 4-OH (δ_H 3.79, d, J = 12.0 Hz) and H-4 implied that rotation around the C-4/O bond was restricted due to a hydrogen bond between 4-OH and the C-18 carbonyl. This required that C-18 and 4-OH were oriented on the same face of the cyclopentane ring in **1**; thus, the relative configuration at C-2 was assigned as *R**. The geometry of the exocyclic C-1/C-9 double bond was suggested to be *E* based on the

deshielded chemical shift of H-9 (δ_H 7.33, s) and the absence of any NOE correlations between H-9/H-3, H-9/H-7, or H-9/H_3-20. With these data, it was possible to propose the constitution and configuration of **1**, but a more rigorous analysis was needed.

Advances in DFT calculations and anisotropic NMR methods provided the means to orthogonally verify both the structure and relative stereochemistry of **1**.[3,4] The ^{1}H and ^{13}C chemical shifts of four isomers, a pair of diastereomers with different stereochemistry at the C-2 spiro carbon and the *E*/*Z* isomers of the 1-ene, i.e., 1*E*,2*S* (**1a**), 1*Z*,2*S* (**1b**), 1*E*,2*R* (**1c**), and 1*Z*,2*R* (**1d**), were calculated by DFT[9] at the mPW1PW91/6–311+G(2d,p)//M06–2X/6–31+G(d,p) level of theory. The results (Table 1) indicated that the root-mean-square deviation (RMSD) and mean absolute error (MAE) values of the calculated ^{1}H chemical shifts of **1a**, **1b**, and **1c** were very similar (0.16 and 0.12–0.13 ppm, respectively), while RMSD and MAE for **1d** were significantly higher (0.33 and 0.21 ppm, respectively). Thus, on the basis of calculated ^{1}H chemical shifts, the stereochemistry remained ambiguous. Conversely, the RMSD and MAE of the calculated ^{13}C chemical shifts gave better differentiating power, suggesting **1c** as the best candidate, but the difference between the ^{13}C RMSD of **1a** and **1c** (~0.4 ppm) was not significant enough to draw an unambiguous conclusion. For a more rigorous chemical shift analysis DP4+ was utilized.[10] Using only ^{1}H chemical shifts, the DP4+ analysis again afforded ambiguous results, but when ^{13}C chemical shifts were incorporated the results clearly favored **1c** as the correct isomer. However, the rather high ^{13}C RMSD observed for all four isomers (1.91–2.65 ppm), coupled with the fact that both **1a** and **1c** have similar DP4+ probabilities when using only ^{1}H data, led us to conclude that stereochemical discrimination could not be considered definitive. Since DP4+ can sometimes produce false positives, we utilized anisotropic NMR methods to provide orthogonal confirmation of the stereochemistry at the spiro carbon and the exocyclic olefin.

RCSA data can provide key stereochemical discrimination for quaternary carbons;[11] hence, the RCSA values of **1** were measured using PBLG [poly-γ-(benzyl-L-glutamate)] as the alignment medium,[12] and the chemical shift anisotropy tensors were calculated for all four isomers **1a**, **1b**, **1c**, and **1d**. Upon inspection of the 3D structures of the lowest energy conformers of each isomer (cutoff was set to ≥2% Boltzmann population) obtained from the DFT calculations, we observed that the core of the molecule was conformationally rigid, allowing a high degree of alignment among the selected superimposed conformers if the flexible side chains were not included in the analysis (Supporting Information). Thus, *Q* factors for each isomer were calculated using single tensor fitting of the experimental RCSA values of C-1–C-6, C-9–C-12, and C-17–C-20 vs the back-calculated RCSA values for the lowest energy conformer of each respective isomer. As illustrated in Figure 2, the lowest *Q* factor was obtained for isomer 1*E*,2*R* (**1c**) with a value of 0.097, followed by 1*Z*,2*S* (**1b**) with a *Q* factor of 0.138 (ratio **1b**/**1c** = 1.423), 1*E*,2*S* (**1a**) with a *Q* factor of 0.196 (ratio **1a**/**1c** = 2.021) and 1*Z*,2*R* (**1d**) with a *Q* factor of 0.234 (ratio **1d**/**1c** = 2.412). These RCSA results further support that **1c** is the correct structure for dictyospiromide, providing orthogonal evidence of the relative stereochemistry at the spiro carbon and the 1-ene double bond. The combined application of RCSA measurements, DFT chemical shift calculations, and analysis of proton coupling constant and NOE data provided consistent and complementary verification of the constitution and configuration of **1**.

The absolute configuration at C-4 was determined by in situ generation of a metal-complexed auxiliary chromophore after addition of $Rh_2(OCOCF_3)_4$ to a $CHCl_3$ solution of **1** and measurement of the induced CD (ICD) spectrum. The sign of the E band (350 nm) in the ICD spectrum is indicative of the absolute configuration of secondary alcohols by applying Snatzke's bulkiness rule;[13] thus, the negative Cotton effect observed at 350 nm (Supporting Information) was in agreement with a 4*R* configuration. With these findings in hand, the absolute configurations at C-2, C-3, C-6, and C-10 were established as *R*, *S*, *S*, and *R*, respectively. Support for this assignment was provided by comparison of the experimentally recorded ECD spectrum of dictyospiromide (**1**) with DFT-calculated ECD spectra at the B3LYP/def2-TZVP level of theory for the four isomers of **1** [**1a** (1*E*,2*S*), **1b** (1*Z*,2*S*), **1c** (1*E*,2*R*), and **1d** (1*Z*,2*R*)]. The measured ECD spectrum of **1** was very similar to the calculated spectrum for **1c** (Figure 3).

Cells in aerobic environments have to contend with reactive oxygen species (ROS) and the resultant oxidative damage they produce, so numerous oxidative stress response mechanisms have evolved, including the production of antioxidant secondary metabolites. The cytoprotective effect of dictyospiromide (**1**) against H_2O_2-induced oxidative damage and toxicity in neuron-like PC12 cells was evaluated, and cell survival following treatment with **1** increased in a dose-dependent manner (Figure 4a). This was coupled with a reduction in H_2O_2-induced lactate dehydrogenase (LDH) production in cells treated with **1** at a concentration as low as 0.5 μM (Figure 4b). Release of LDH is an index of cell injury; thus, **1** is a potent cytoprotectant with antioxidant properties. Compound **1** was also investigated for activation of the Nrf2/ARE signaling pathway, which regulates the expression of genes involved in cellular antioxidant defense and is recognized as an important mediator of neuroprotection. The effect of **1** on nuclear translocation of Nrf2 was assessed, and both **1** (2 μM) and the positive control *tert*-butylhydroquinone (TBHQ, 2 μM) significantly enhanced accumulation of Nrf2 in the nucleus (Figure 4c), suggesting that **1** is a potent Nrf2 activator. In a Western blot assay for up-regulation of heme oxygenase-1 (HO-1) expression, an antioxidant protein regulated by Nrf2, **1** promoted HO-1 production in a dose-dependent manner comparable to that of TBHQ (Figure 4d). Nrf2 siRNA was applied to investigate if the antioxidant effect of **1** in PC12 cells is dependent on Nrf2. Cell viability in the control siRNA group (si Con) was increased by **1**, while the cytoprotection was reversed by knockdown of Nrf2 (Figure 4e), indicating that Nrf2 contributes to the antioxidant effect of **1**. Finally, the role of HO-1 in the cytoprotective effect of **1** was investigated using the HO-1 inhibitor zinc protoporphyrin (ZnPP). Cytoprotection provided by **1** was partially suppressed when **1** and the maximum noncytotoxic concentration of ZnPP were applied together, implying that HO-1 contributes to the antioxidant activity of **1** (Figure 4f). Thus, dictyospiromide (**1**) demonstrated a cytoprotective antioxidant effect in PC12 cells that involved activation of the Nrf2/ARE signaling pathway and enhanced expression of HO-1.

In summary, combined application of contemporary spectroscopic and computational methods allowed unambiguous assignment of the constitution and configuration of the novel marine alkaloid dictyospiromide (**1**). Anisotropic NMR experiments provided orthogonal evidence for defining the stereochemistry of the difficult to define spiro ring junction and exocyclic olefin. Dictyospiromide (**1**) showed potent cytoprotective and antioxidant

properties associated with activated Nrf2/ARE signaling, so its novel molecular scaffold could serve as a lead structure for the development of neuroprotective agents that reduce cellular oxidative stress.

Supplementary Material

Refer to Web version on PubMed Central for supplementary material.

ACKNOWLEDGMENTS

This work was supported in part by the Natural Science Foundation of Zhejiang Province, China (No. LQ19H300003; Y19B020043), Public Project of Zhejiang Province (No. 2017C37042), Outstanding Youth Foundation from Wenzhou Medical University (No. 604091809), the Opening Project of Zhejiang Provincial Top Key Discipline of Pharmaceutical Sciences (No. 201707), and the Intramural Research Program of the NIH, National Cancer Institute, Center for Cancer Research.

REFERENCES

(1). (a)Adams RW Pure Shift NMR Spectroscopy. eMagRes 2014, 3 (4), 1–15.(b)Castañar L; Parella T Broadband ^{1}H Homodecoupled NMR Experiments: Recent Developments, Methods and Applications. Magn. Reson. Chem 2015, 53 (6), 399–426. [PubMed: 25899911] (c)Williamson RT; Buevich AV; Martin GE; Parella T LR-HSQMBC: A Sensitive NMR Technique to Probe Very Long-Range Heteronuclear Coupling Pathways. J. Org. Chem 2014, 79 (9), 3887–3894. [PubMed: 24708226] (d)Saurí J; Bermel W; Buevich AV; Sherer EC; Joyce LA; Sharaf MHM; Schiff PL Jr.; Parella T; Williamson RT; Martin GE Homodecoupled 1,1- and 1,n-ADEQUATE: Pivotal NMR Experiments for the Structure Revision of Cryptospirolepine. Angew. Chem., Int. Ed 2015, 54 (35), 10160–10164.(e)Saurí J; Marcó N; Williamson RT; Martin GE; Parella T Extending Long-Range Heteronuclear NMR Connectivities by HSQMBC-COSY and HSQMBC-TOCSY Experiments. J. Magn. Reson 2015, 258, 25–32. [PubMed: 26160012]

(2). (a)Rovnyak D; Sarcone M; Jiang Z Sensitivity Enhancement for Maximally Resolved Two-Dimensional NMR by Nonuniform Sampling. Magn. Reson. Chem 2011, 49 (8), 483–491. [PubMed: 21751244] (b)Palmer MR; Suiter CL; Henry GE; Rovnyak J; Hoch JC; Poloneva T; Rovnyak D Sensitivity of Nonuniform Sampling NMR. J. Phys. Chem. B 2015, 119 (22), 6502–6515. [PubMed: 25901905]

(3). (a)Nath N; Schmidt M; Gil RR; Williamson RT; Martin GE; Navarro-Vázquez A; Griesinger C; Liu Y Determination of Relative Configuration from Residual Chemical Shift Anisotropy. J. Am. Chem. Soc 2016, 138 (30), 9548–9556. [PubMed: 27294984] (b)Liu Y; Saurí J; Mevers E; Peczuh MW; Hiemstra H; Clardy J; Martin GE; Williamson RT Unequivocal Determination of Complex Molecular Structures Using Anisotropic NMR Measurements. Science 2017, 356, 43. (c)Liu Y; Navarro-Vázquez A; Gil RR; Griesinger C; Martin GE; Williamson RT Application of Anisotropic NMR Parameters to the Confirmation of Molecular Structure. Nat. Protoc 2019, 14, 217–247. [PubMed: 30552410] (d)Navarro-Vázquez A; Gil RR; Blinov K Computer-Assisted 3D Structure Elucidation (CASE-3D) of Natural Products Combining Isotropic and Anisotropic NMR Parameters. J. Nat. Prod 2018, 81 (1), 203–210. [PubMed: 29323895] (e)Mevers E; Saurí J; Liu Y; Moser A; Ramadhar TR; Varlan M; Williamson RT; Martin GE; Clardy J; Homodimericin A A Complex Hexacyclic Fungal Metabolite. J. Am. Chem. Soc 2016, 138 (38), 12324–12327. [PubMed: 27608853] (f)Milanowski DJ; Oku N; Cartner LK; Bokesch HR; Williamson RT; Saurí J; Liu Y; Blinov KA; Ding Y; Li X-C; Ferreira D; Walker LA; Khan S; Davies-Coleman MT; Kelley JA; McMahon JB; Martin GE; Gustafson KR Unequivocal Determination of Caulamidines A and B: Application and Validation of New Tools in the Structure Elucidation Tool Box. Chem. Sci 2018, 9 (2), 307–314. [PubMed: 29619201]

(4). (a)Lodewyk MW; Siebert MR; Tantillo DJ Computational Prediction of ^{1}H and ^{13}C Chemical Shifts: A Useful Tool for Natural Product, Mechanistic, and Synthetic Organic Chemistry. Chem. Rev 2012, 112 (3), 1839–1862. [PubMed: 22091891] (b)Lodewyk MW; Soldi C; Jones PB; Olmstead MM; Rita J; Shaw JT; Tantillo DJ The Correct Structure of Aquatolide-Experimental

Validation of a Theoretically-Predicted Structural Revision. J. Am. Chem. Soc 2012, 134 (45), 18550–18553. [PubMed: 23101682] (c)Tantillo DJ Walking in the Woods with Quantum Chemistry – Applications of Quantum Chemical Calculations in Natural Products Research. Nat. Prod. Rep 2013, 30, 1079–1086. [PubMed: 23793561] (d)Grimblat N; Sarotti AM Computational Chemistry to the Rescue: Modern Toolboxes for the Assignment of Complex Molecules by GIAO NMR Calculations. Chem. - Eur. J 2016, 22 (35), 12246–12261. [PubMed: 27405775] (e)Zanardi MM; Sarotti AM GIAO C–H COSY Simulations Merged with Artificial Neural Networks Pattern Recognition Analysis. Pushing the Structural Validation a Step Forward. J. Org. Chem 2015, 80 (19), 9371–9378. [PubMed: 26339863] (f)Kutateladze AG; Reddy DS High-Throughput in Silico Structure Validation and Revision of Halogenated Natural Products Is Enabled by Parametric Corrections to DFT-Computed ^{13}C NMR Chemical Shifts and Spin–Spin Coupling Constants. J. Org. Chem 2017, 82 (7), 3368–3381. [PubMed: 28339201]

(5). (a)Krivdin LB Theoretical Calculations of Carbon-Hydrogen Spin-Spin Coupling Constants. Prog. Nucl. Magn. Reson. Spectrosc 2018, 108, 17–73. [PubMed: 30538048] (b)Buevich AV; Saurí J; Parella T; De Tommasi N; Bifulco G; Williamson RT; Martin GE Enhancing the Utility of $^{1}J_{CH}$ Coupling Constants in Structural Studies Through Optimized DFT Analysis. Chem. Commun 2019, 55, 5781–5784.(c)Krivdin LB Carbon-Carbon Spin-Spin Coupling Constants: Practical Applications of Theoretical Calculations. Prog. Nucl. Magn. Reson. Spectrosc 2018, 105, 54–99. [PubMed: 29548367] (d)Navarro-Vázquez A State of the Art and Perspectives in the Application of Quantum Chemical Prediction of ^{1}H And ^{13}C Chemical Shifts and Scalar Couplings for Structural Elucidation of Organic Compounds. Magn. Reson. Chem 2017, 55 (1), 29–32. [PubMed: 27531665] (e)Kutateladze AG; Mukhina OA Relativistic Force Field: Parametrization of ^{13}C–^{1}H Nuclear Spin–Spin Coupling Constants. J. Org. Chem 2015, 80 (21), 10838–10848. [PubMed: 26414291] (f)Buevich AV; Elyashberg ME Synergistic Combination of CASE Algorithms and DFT Chemical Shift Predictions: A Powerful Approach for Structure Elucidation, Verification, and Revision. J. Nat. Prod 2016, 79 (12), 3105–3116. [PubMed: 28006916]

(6). Joyce LA; Nawrat CC; Sherer EC; Biba M; Brunskill A; Martin GE; Cohen RD; Davies IW Beyond Optical Rotation: What's Left is not Always Right in Total Synthesis. Chem. Sci 2018, 9 (2), 415–424. [PubMed: 29629112]

(7). Hallwass F; Schmidt M; Sun H; Mazur A; Kummerlöwe G; Luy B; Navarro-Vázquez A; Griesinger C; Reinscheid UM Residual Chemical Shift Anisotropy (RCSA): A Tool for the Analysis of the Configuration of Small Molecules. Angew. Chem., Int. Ed 2011, 50 (40), 9487–9490.

(8). Chen J; Li H; Zhao Z; Xia X; Li B; Zhang J; Yan X Diterpenes from the Marine Algae of the Genus Dictyota. Mar. Drugs 2018, 16 (5), 159–184.

(9). (a)Lodewyk MW; Siebert MR; Tantillo DJ Computational Prediction of ^{1}H and ^{13}C Chemical Shifts: A Useful Tool for Natural Product, Mechanistic, and Synthetic Organic Chemistry. Chem. Rev 2012, 112 (3), 1839–1862. [PubMed: 22091891] (b)Pierens GK ^{1}H and ^{13}C NMR Scaling Factors for the Calculation of Chemical Shifts in Commonly Used Solvents Using Density Functional Theory. J. Comput. Chem 2014, 35 (18), 1388–1394. [PubMed: 24854878]

(10). (a)Smith SG; Goodman JM Assigning Stereochemistry to Single Diastereoisomers by GIAO NMR Calculation: The DP4 Probability. J. Am. Chem. Soc 2010, 132 (37), 12946–12959. [PubMed: 20795713] (b)Grimblat N; Zanardi MM; Sarotti AM Beyond DP4: An Improved Probability for the Stereochemical Assignment of Isomeric Compounds Using Quantum Chemical Calculations of NMR Shifts. J. Org. Chem 2015, 80 (24), 12526–12534. [PubMed: 26580165]

(11). Ndukwe IE; Brunskill A; Gauthier DR Jr.; Zhong YL; Martin GE; Williamson RT; Reibarkh M; Liu Y ^{13}C NMR-Based Approaches for Solving Challenging Stereochemical Problems. Org. Lett 2019, 21 (11), 4072–4076. [PubMed: 31117703]

(12). Liu Y; Cohen RD; Gustafson KR; Martin GE; Williamson RT Enhanced Measurement of Residual Chemical Shift Anisotropy for Small Molecule Structure Elucidation. Chem. Commun 2018, 54 (34), 4254–4257.

(13). Gerards M; Snatzke G Circular Dichroism, XCIII[1] Determination of the Absolute Configuration of Alcohols, Olefins, Epoxides, and Ethers from the CD of Their "In Situ" Complexes With $[Rh_2(O_2CCF_3)_4]$. Tetrahedron: Asymmetry 1990, 1 (4), 221–236.

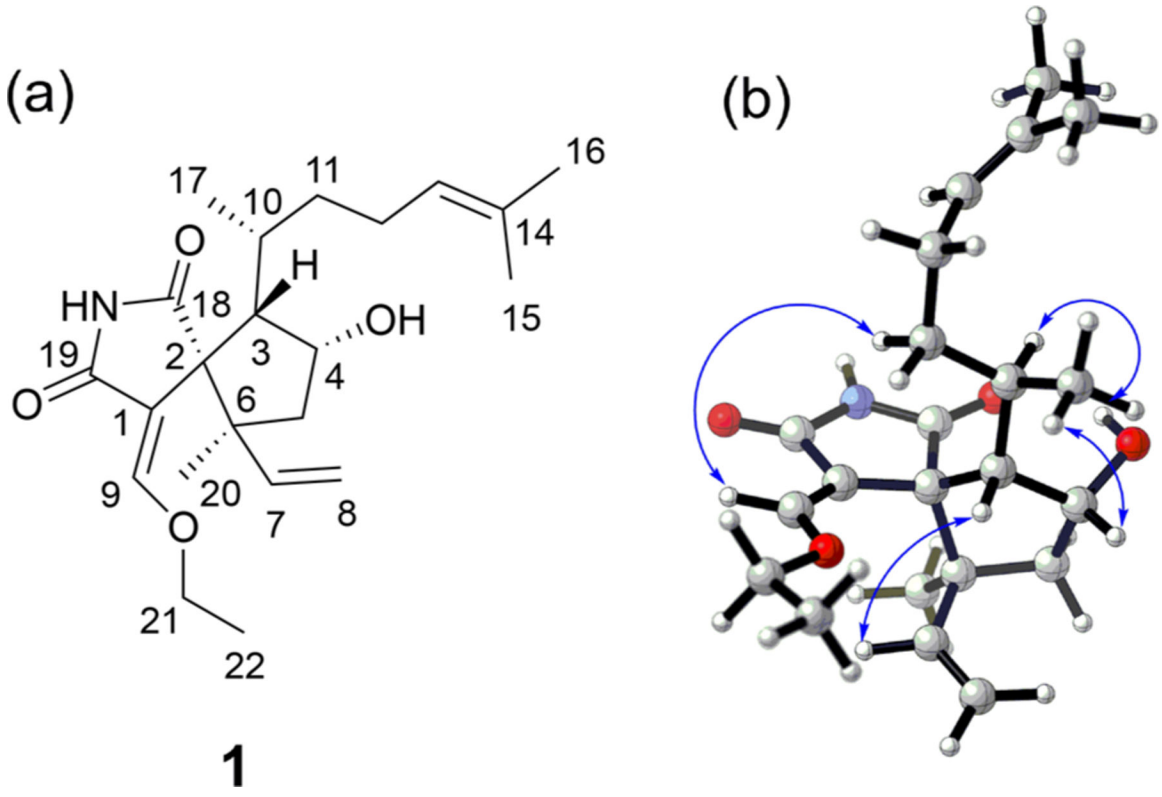

Figure 1.
(a) Structure of dictyospiromide (**1**) and (b) key NOEs.

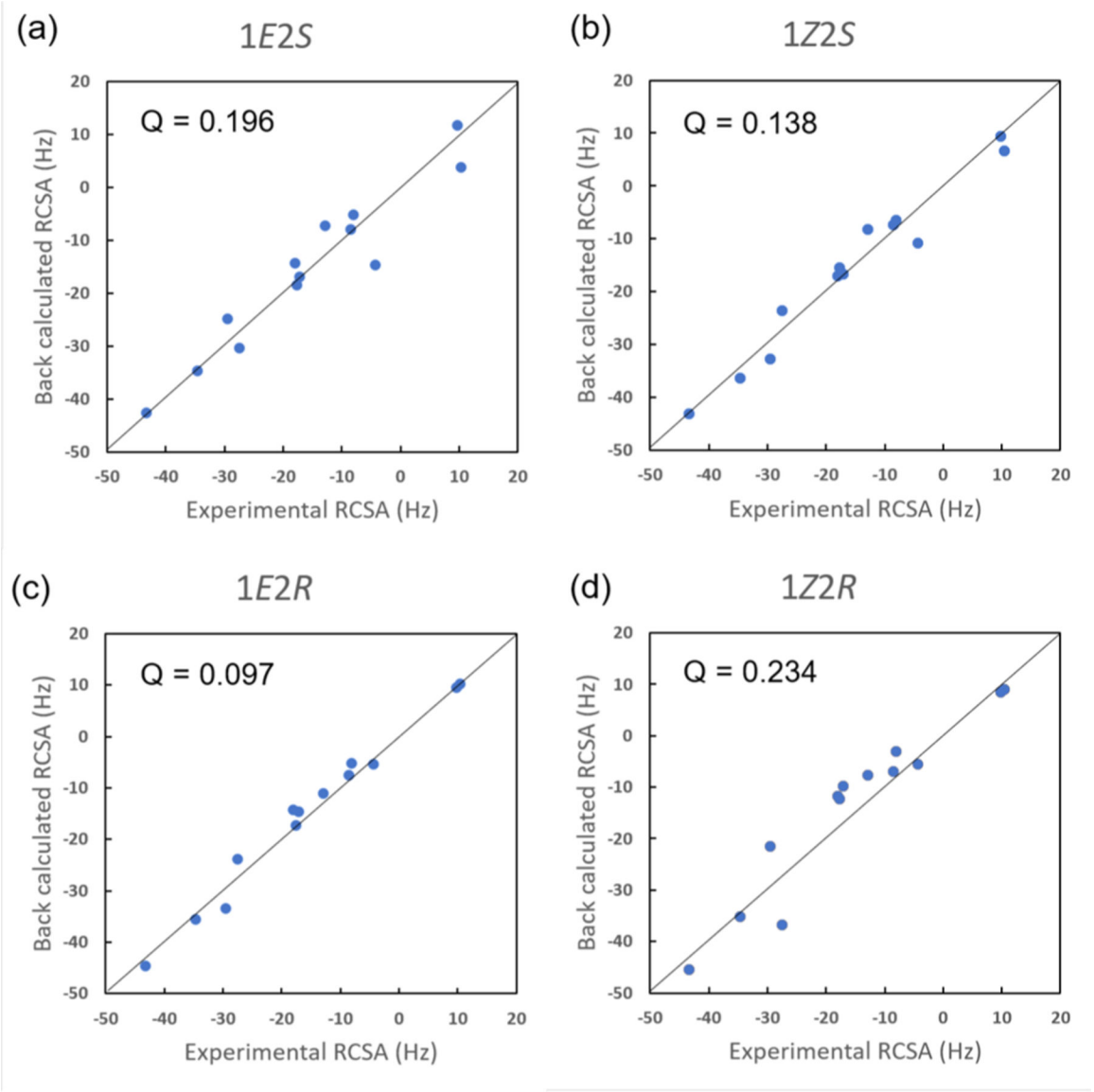

Figure 2.

Back-calculated vs experimentally measured ^{13}C RCSA values for the (a) **1a**, (b) **1b**, (c) **1c**, and (d) **1d** isomers.

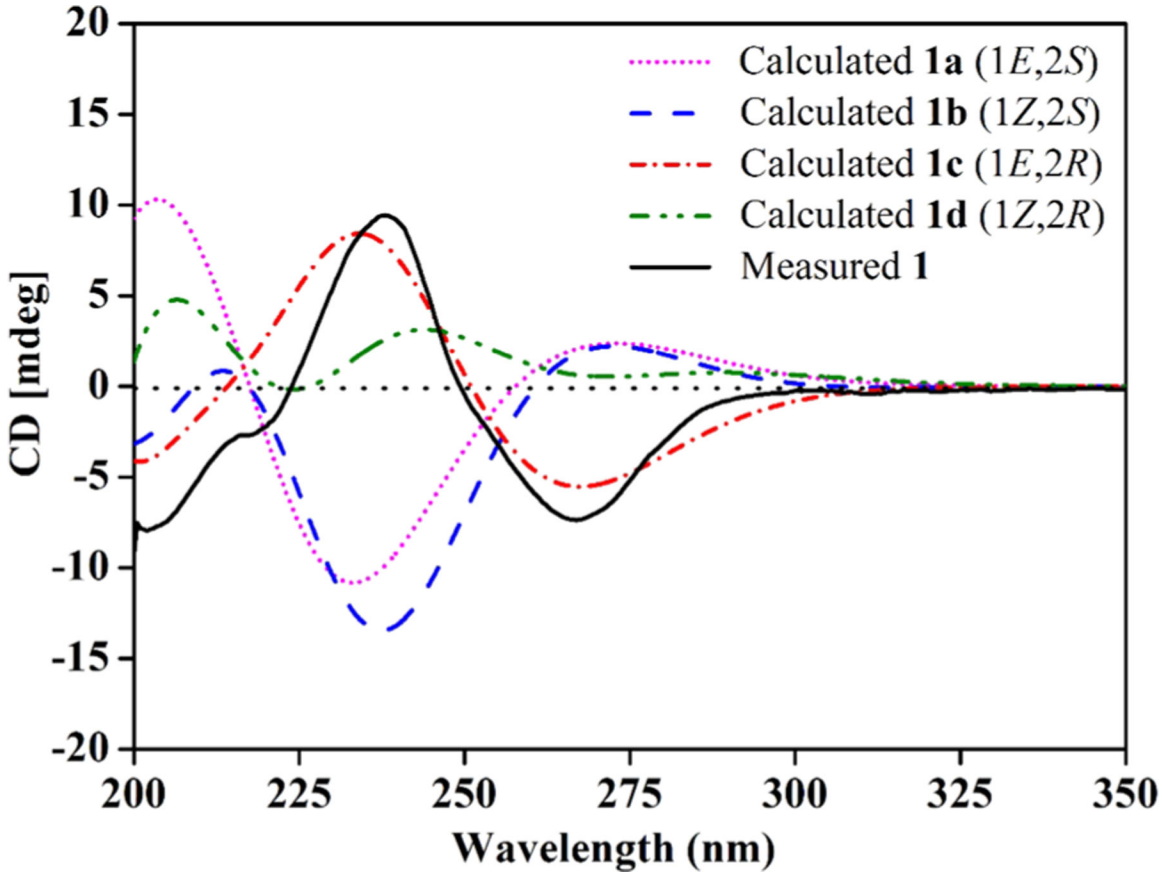

Figure 3.

ECD spectrum of dictyospiromide (**1**) and calculated ECD spectra of four possible configurations **1a** (1*E*, 2*S*), **1b** (1*Z*, 2*S*), **1c** (1*E*, 2*R*), and **1d** (1*Z*, 2*R*).

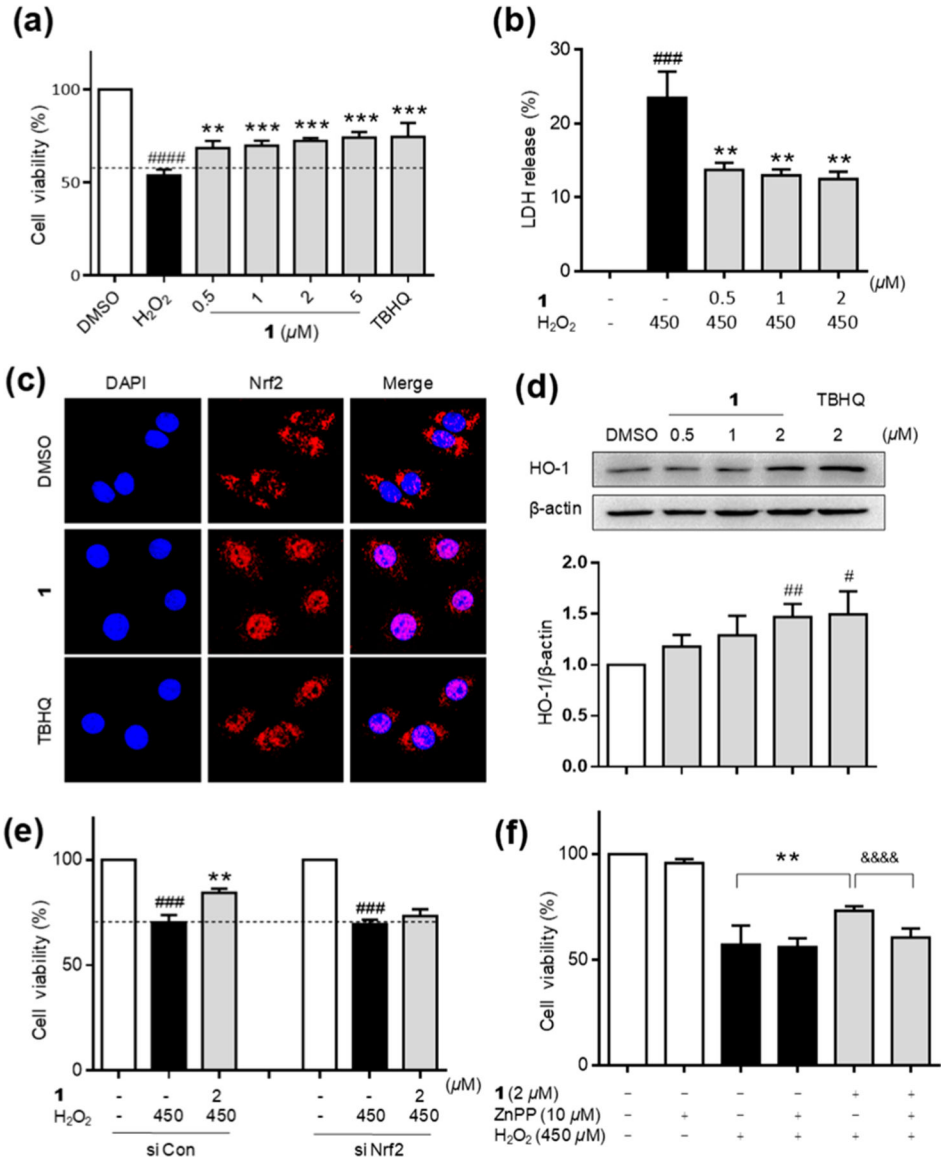

Figure 4.

Dictyospiromide (**1**) protects PC12 cells from oxidative damage by activating the Nrf2 signaling pathway. (a) **1** increased cell survival in a H_2O_2 damage model. TBHQ (2 μM) was used as the positive control. (b) **1** decreased LDH production after treatment with H_2O_2. (c) **1** induced Nrf2 nuclear translocation in cells stained with DAPI (blue) and Nrf2 antibody (red). (d) **1** up-regulated the expression of HO-1 protein in PC12 cells. (e) Down-regulation of Nrf2 expression by siRNA decreased the cytoprotective effect of **1**. (f) Pretreatment with HO-1 inhibitor ZnPP suppressed the cytoprotective effects of **1**.

Table 1.

Summary of DFT Chemical Shift RMSD and MAE Values Obtained for 1a–1d and DP4+ Probabilities for the Isomers

	1a: 1*E*,2*S*	**1b: 1*Z*,2*S***	**1c: 1*E*,2*R***	**1d: 1*Z*,2*R***
^{1}H RMSD (ppm)	0.16	0.16	0.16	0.33
^{1}H MAE (ppm)	0.12	0.13	0.12	0.21
^{13}C RMSD (ppm)	2.29	2.44	1.91	2.65
^{13}C MAE (ppm)	1.74	1.74	1.34	1.93
DP4+ (^{1}H) (%)	43.03	4.01	52.96	0
DP4+ (^{13}C) (%)	0.06	0.06	99.88	0
DP4+ (^{1}H + ^{13}C) (%)	0.05	0	99.95	0